Translational Oncology
www.transonc.com

Volume 4 Number 4 August 2011 pp. 249–257 249

Antitumor Efficacy of a Thrombospondin 1 Mimetic CovX-Body

Lingna Li, Tom A. Leedom, Janet Do, Hanhua Huang, JingYu Lai, Kim Johnson, Trina F. Osothprarop, John D. Rizzo, Venkata R. Doppalapudi, Curt W. Bradshaw, Rodney W. Lappe, Gary Woodnutt, Nancy J. Levin and Steven R. Pirie-Shepherd

CovX Research LLC, San Diego, CA, USA

Abstract

CVX-045 is produced by covalently attaching a thrombospondin 1 (TSP-1) mimetic comprising a peptidic sequence and a linker to the Fab binding site of a proprietary scaffold antibody. CVX-045 possesses the potency of the TSP-1–derived peptide, along with the advantageous pharmacokinetics of an antibody. Antitumor activity of CVX-045 was evaluated in human xenograft models alone and in combination with standard chemotherapies and targeted molecules. In A549 and A431 xenograft models, CVX-045 demonstrated significant ($P < .05$) antiangiogenic activity, reducing tumor microvessel density and increasing the levels of necrosis within treated tumors. In an HT-29 xenograft model, CVX-045 in combination with 5-fluorouracil significantly ($P < .01$) decreased tumor growth rate compared with vehicle, CVX-045, or 5-fluorouracil alone. Cotreatment of CVX-045 plus CPT-11 delayed progression of tumor growth from day 28 to 60. In contrast CVX-045 alone treatment did not delay the progression of tumor growth, and CPT-11 alone delayed progression of tumor growth to day 39. Cotreatment of CVX-045 with sunitinib extended the time to reach tumor load from day 26 to 40. In summary, CVX-045 exhibits significant antiangiogenic activity in several tumor models and enhances antitumor activity in combination with chemotherapy or targeted therapies. These data suggest future avenues for effective combination therapy in treating solid tumors. CVX-045 has recently completed a phase 1 trial in solid tumors where it has been well tolerated.

Translational Oncology (2011) 4, 249–257

Introduction

Angiogenesis is the process whereby preexisting blood vessels can be induced to sprout, leading to an increase in local vasculature [1]. The process is important in a variety of physiological events such as wound healing and the menstrual cycle in female reproductive organs [2]. The angiogenic process is tightly regulated by both positive and negative effectors [3]. Positive regulators of angiogenesis include vascular endothelial growth factor (VEGF), fibroblast growth factors (FGFs), epidermal growth factor, and hepatocyte growth factor. These factors can induce endothelial cells to migrate, proliferate, or form tube-like structures. There are also several negative regulators of angiogenesis, such as thrombospondin 1 (TSP-1), and small "cryptic" fragments of larger proteins that are intimately involved in coagulation and fibrinolysis [4]. Under normal conditions, angiogenesis is activated and deactivated in a tightly coordinated sequence of events as evidenced, for example, in wound healing [5].

Tumors have been described as "wounds that never heal" [6], in that they upregulate or induce the up-regulation of positive effectors of angiogenesis, but do not balance this process with the expression of negative regulators. In essence, tumors have turned on the angiogenic switch and cannot turn it off, and it has been suggested that the endothelial compartment of a tumor would be a good target for therapeutic intervention [7]. To date, most efforts have attempted to attenuate the effects of the positive regulators through growth factor traps such as Avastin [8] or growth factor receptor antagonists such as Sutent [9]. However, amplifying the effects of known negative regulators of angiogenesis such as TSP-1 also has potential for antiangiogenic intervention.

Address all correspondence to: Steven R. Pirie-Shepherd, PhD, CovX Research LLC, 9381 Judicial Dr, Suite 200, San Diego, CA 92121. E-mail: Steven.pirie-shepherd@pfizer.com
Received 16 March 2011; Revised 10 May 2011; Accepted 11 May 2011

 1944-7124/11/$25.00
DOI 10.1593/tlo.11136

TSP-1 is a 420-kDa matrix protein that not only inhibits adhesion, proliferation, and tube formation by several types of endothelial cells but also inhibits angiogenesis in the chorioallantoic membrane assay [10]. TSP-1 has also been used to successfully treat cancer in a mouse model [11]. However, the use of TSP-1 as an antiangiogenic drug in humans is prohibitive owing to both its size and multiple other biologic activities.

TSP-1 is a trimer, with each promoter composed of multiple domains including three types of sequence motifs (type 1, 2, and 3 repeats [12]). TSP-1 has three type 1 repeat (TSR) domains. Within the TSR domains, the sequence GVITRIR seems to demonstrate antiangiogenic activity with the adjacent sequence CSVTCG, providing some form of enhancement of activity [13]. Peptides based on the GVITRIR sequence of TSR have been reported to inhibit the migration of endothelial cells and have been used successfully to treat metastatic tumors in syngeneic mouse models as well as orthotopic bladder tumors in immune-deficient mice [14]. However, both tumor models required twice-daily administration of the TSP-1–derived peptide.

It is all too common for bioactive compounds with excellent anticancer efficacy *in vitro* to fail in the clinic because of a requirement for therapy-intensive treatment regimens. We show here that a TSP-1 mimetic pharmacophore with potent antiangiogenic activity can be combined with a proprietary reactive monoclonal antibody to create a CovX-Body termed *CVX-045*. We describe here the efficacy of CVX-045 administered as a monotherapy in tumor xenografts and in combination with chemotherapy or targeted therapy such as that including irinotecan, 5-fluorouracil (5-FU), and Sutent. CVX-045 significantly reduces microvessel density, induces apoptosis, and increases the necrotic core of treated tumors. CVX-045 has recently completed a phase 1 trial [15]. The data provided here suggest possible combinations for a phase 2 trial that would enable additive antitumor and antiangiogenic effects.

Materials and Methods

Drugs

Sunitinib was obtained from Biomol International (Plymouth Meeting, PA), and CPT-11 and 5-FU were obtained from Henry Schein (Melville, NY).

Production of CVX-045

The synthesized pharmacophore (azetidinone-PEG-Pro-Gly-Val-(D-alloIle)-Thr-Nva-Ile-Arg-Pro-NHEt) was programmed at a 4:1 ratio (pharmacophore/Ab) at 25°C for 24 hours. After programming, free pharmacophore was removed using gel filtration (PD-10 column; 17-0851-01; Amersham, Piscataway, NJ). The final protein concentration was determined by monitoring the absorbance at 280 nm, and programming efficiency was confirmed by mass spectrometry analysis of the column-purified dosing solution. Dosing solution was diluted to working concentrations with phosphate-buffered saline (PBS). All dosing solutions were prepared fresh 1 or 2 days before dosing and stored at 4°C until use.

Endothelial Cell Migration

Endothelial cell migration was performed as described [16]. Human dermal microvascular endothelial cells (Cambrex, Walkersville, MD) and bovine adrenal microvascular endothelial cells (VEC Technologies, Rensselaer, NY) were grown in VEC endothelial cell complete medium. Confluent (80%-90%) endothelial cells were starved overnight in endothelial basal medium (EBM)/bovine serum albumin (BSA; Cambrex, Walkersville, MD) containing 0.1% BSA (Sigma, St Louis, MO). Cells were then harvested with trypsin/EDTA (0.05%; Mediatech, Herndon, VA) and resuspended in EBM/BSA at a concentration of 1.5 to 2.0 × 10^6 cells/ml. Cells (29 μl) were added to the bottom of a modified Boyden chamber (Nucleopore, Gaithersburg, MD) and covered with gelatinized PVDF Nucleopore membrane (Whatman, Florham Park, NJ), placed with the milky side facing the cells and shiny side away from the cells. The chambers were assembled and inverted, and the cells were allowed to adhere for 90 minutes at 37°C. Recombinant human basic fibroblast growth factor (bFGF; 20 ng/ml; R&D Systems, Minneapolis, MN) or 0.25% to 0.5% fetal bovine serum (FBS; Tissue Culture Biologicals, Tulare, CA) were used for a positive control as indicated, and EBM/BSA was used for a negative control. EBM/BSA, inducers (20 ng/ml bFGF or 0.25% FBS, prepared in EBM/BSA), and TSP-1 (Calbiochem, San Diego, CA) (20 nM) + inducer were also included in each chamber to monitor the success of the assay. Background migration was subtracted, and the data presented as a percentage of bFGF or FBS-induced migration (% maximal migration) ± SEM.

General Animal Methods

Young adult female *Nu-Foxn1^{nu}* mice (Charles River Laboratories, Wilmington, MA) were housed 5 to 10 per cage in a temperature- and light-controlled vivarium (lights on-off 12:12 hours) with standard laboratory chow and water available *ad libitum*. All husbandry materials were sterilized by autoclaving. Mice were allowed to rest undisturbed for at least 48 hours after arrival before experimentation was initiated. All animal experiments were conducted after protocol approval by the CovX Institutional Animal Care and Use Committee.

Matrigel Plug Assay

Growth factor–reduced Matrigel (catalog no. 354230; BD Biosciences, San Diego, CA) was brought to the liquid phase by placing on ice for several hours. Recombinant human bFGF (catalog no. 356060; BD Biosciences) was added to the Matrigel to a final concentration of 100 ng/ml. The Matrigel was loaded into prechilled syringes that were held on ice to maintain the material in the liquid state for injection.

Mice (*Nu-Foxn1^{nu}*) were anesthetized by isoflurane inhalation for subcutaneous injection of the Matrigel (0.5 ml/mouse) in the upper abdominal region. In initial studies, treatment was initiated 3 to 4 hours later on the same day. Five mice were randomly assigned to each treatment group, and treatment (0.1-1 mg/kg administered intravenously in 0.2 ml of PBS) was given once on day 0 and Matrigel plugs and were allowed to mature for 7 days. At the end of the 7-day period, mice were killed by CO_2 asphyxiation and Matrigel implants ("plugs") were carefully dissected free of surrounding tissue.

Quantification of Angiogenesis in the Matrigel Plug

Implants were snap frozen on liquid nitrogen and embedded in OCT, and frozen 5-μm sections were prepared on a cryostat. Three- to five-step sections (5 μm every 30 μm) were mounted on slides and fixed by routine histologic procedures. CD31 immunoreactivity was localized using a rat antimouse CD31 antibody (catalog no. 550274; BD Pharmingen, San Diego, CA) and detected using an antirat IgG–horseradish peroxidase (HRP) detection kit (catalog no. 551013; BD Pharmingen). Slides were then photographed and CD31-immunopositive

staining of the images was quantified using ImagePro 5.1 software. Total CD31 immunoreactivity was summed over all five sections for each Matrigel implant and expressed as pixels per plug. All analyses were conducted by operators blinded to the treatment groups.

Pharmacokinetics Studies

The pharmacokinetics (PK) of CVX-045, were determined in male Swiss Webster mice (Charles River Laboratories). Mice were dosed with CovX-Bodies at 10 mg/kg intravenously; blood samples from three mice per time point were taken at 0.08, 0.25, 0.5, 1, 2, 4, 6, and 24 hours; and serum samples were prepared by centrifugation. CVX-045 concentrations were determined using a rabbit polyclonal antibody generated against the TSP-1 peptidomimetic portion of CVX-045 in a capture ELISA. In brief, plates were coated with anti-peptidomimetic antibody, and serum samples added. The Fc portion of CVX-045 was then detected by the addition of HRP-conjugated donkey antihuman IgG (Bethyl Laboratories, Montgomery, TX) and TMB developing solution (Kirkegaard and Perry Laboratories, Gaithersburg, MD).

Xenograft Tumor Studies

Tumor cell lines were cultured in RPMI 1640 medium with 10% FBS in a 5% CO_2 incubator with 98% humidity. Subconfluent cells (70%-80%) were harvested after brief treatment with 0.25% trypsin and resuspended in Hank's balanced salt solution for inoculation.

Tumor cell suspensions (3-5 × 10^6 cells, depending on the cell line) were injected SC in a volume of 0.2 ml into the right flank of each mouse. In studies where drug was administered concurrently with tumor inoculation, 8 to 10 mice were randomly assigned to each treatment group, and treatments were conducted for up to 4 weeks. In all other studies, treatments were initiated the day after tumor inoculation and continued for up to 4 weeks. Tumor measurements were made periodically with manual calipers at least weekly, and tumor volumes were calculated using the formula: 0.52 × length × $width^2$. At the end of the study, tumors were excised and weighed, and then for some studies, tumors were analyzed (immuno)histochemically. In studies where tumors were staged, tumor measurements were made with manual calipers at least weekly, and once the required average tumor volume was attained, animals were randomized into groups of 8 to 10, and treatment was initiated within 24 hours. For pseudomortality study designs, each group was killed as the tumor mean volume reached either 1000 or 2000 mm^3.

Quantification of Viable Tumor Area

A ~3-mm section through the midportion of each tumor was fixed in formalin and paraffin embedded. Five-micrometer sections were prepared on a microtome and mounted on slides. Sections were stained with H&E following standard histologic procedures and then photographed using a QImaging MicroPublisher 5.0 RTV camera (Burnaby, British Columbia, Canada) coupled with a Nikon Eclipse 80i microscope (2×; Nikon, Melville, NY). An adjacent cross section of ~3 mm was frozen on liquid nitrogen and then embedded in OCT for preparation of frozen sections using a cryostat.

To determine necrotic and viable tumor area, whole field images of each stained tumor section were acquired at low magnification. ImagePro 5.1 software or ImageJ software (National Institutes of Health, Bethesda, MD) was used to quantify the necrotic and viable area by using the tracing function of measurement. For each tumor tissue, two to five measurements were collected and exported to a Microsoft Excel file (Microsoft Corp, Redmond, WA). The percentage of viable tissue area was calculated as the following formula: viable area (%) = [total tissue area – necrotic area] / total tissue area. All photography and image analysis was conducted by operators blinded to the treatment groups.

Quantification of Microvessel Density

Snap-frozen tumor sections were oriented and embedded in OCT blocks. Three 5-μm sections (one section every 150 μm) were obtained from each block using a Leica CM1850 Cryostat, Buffalo Grove, IL. The slides were immediately fixed in cold acetone for 2 minutes and air-dried. CD31 immunohistochemical staining of blood vessels was carried out using an antirat IgG-HRP detection kit (catalog no. 551013; BD Pharmingen) and followed the methods in the kit's instruction manual. The CD31 antibody (catalog no. 550274; BD Pharmingen) was diluted 1:200. The CD31-positive area in each tumor was imaged using a Qimaging Micropublisher 5.0 RTV camera coupled with a Nikon Eclipse 80i microscope (20×). Five evenly spaced images were taken along a cross section of each tumor starting and ending at a point on the viable rim in which CD31 staining was greatest. ImagePro 5.1 software was used to quantify the CD31-positive area using a common quantitative macro throughout the experiment. CD31-positive pixels/per 20× microscopic field was calculated by dividing the total CD31-positive area of the three sections of each tumor by 15 (five fields from each of three sections from each tumor). All analyses were conducted by operators blinded to the treatment groups.

Quantification of Apoptosis

Tumor frozen sections (5 μm thickness) were processed for double immunofluorescence staining of cleaved caspase 3 and CD31. Slides were treated with an autofluorescence eliminator reagent (catalog no. 2160; Chemicon, Temecula, CA) for 2 minutes and then treated with streptavidin-biotin block (catalog no. SP-2002; Vector Laboratories, Burlingame, CA) for 30 minutes and nonspecific staining block with 2.5% BSA for 15 minutes. Sections were incubated overnight at 4°C with a cocktail of primary antibodies against cleaved caspase 3 (catalog no. 9664 rabbit mAb, diluted 1:100; Cell Signaling Technology, Danvers, MA) and mouse CD31 (rat antimouse CD31, catalog no. 550274, diluted 1:50; BD Pharmingen). The second antibody for cleaved caspase 3 was biotinylated goat-antirabbit IgG (catalog no. PK-6101, diluted 1:200; Vector Laboratories), which was incubated at room temperature for 1 hour. The slides were then treated with a cocktail of Alexa Fluor 555–conjugated strepavidin (catalog no. S32355, diluted 1:400; Invitrogen, Carlsbad, CA) for the detection of cleaved caspase 3 and -labeled polyclonal antirat IgG (catalog no. 554016, diluted 1:100; BD Pharmingen) for CD31, both of which were incubated at room temperature for 1 hour. Sections were rinsed with PBS between each step. After staining the slides were mounted with Antifade with 4′,6-diamidino-2-phenylindole (DAPI) kit (catalog no. 24636; Invitrogen).

Fluorescence images of cleaved caspase 3, CD31, and nuclei were collected using a Nikon fluorescence microscope equipped with appropriate filters and merged using ImagePro 5.1 software. For quantification of apoptosis, three images at 20× microscopic field from each tumor section at the viable rim (area with the most apoptotic cells) were collected and summed. Cleaved caspase 3 immunofluorescence is expressed as pixels per 20× field. All analyses were conducted by operators blinded to the treatment groups.

Quantification of Proliferation

Immmunofluorescence staining of PCNA was carried out on one frozen section (5 μm thickness) of each tumor. Frozen section slides were stained with rabbit anti-PCNA polyclonal antibody (catalog no. ab2426, diluted 1:100; Abcam, Cambridge, MA) overnight at 4°C after treatment with autofluorescence eliminator reagent (catalog no. 2160; Chemicon) for 5 minutes. The second antibody for PCNA used was Alexa Fluor 488–conjugated goat antirabbit IgG (catalog no. A11034, 1:300; Invitrogen) and incubated at room temperature for 1 hour. Sections were rinsed with PBS containing 0.05% Tween 20 between each step. After staining, the slides were mounted with ProLong Gold Antifade reagent with DAPI (catalog no. P36935; Invitrogen) for nuclear staining. Three fluorescence images of PCNA and nuclei from each section were collected using a Qimage Retiga 2000R camera coupled with a Nikon Eclipse 80i fluorescence microscope equipped with tetramethyl rhodamine isothiocyanate/rhodamine, fluorescein isothiocyanate, and DAPI filter cubes, respectively, at each 40× microscopic field. The collected images were then processed, merged, and analyzed using ImagePro 6.1 software. Quantification of proliferation was calculated as percentage of PCNA-positive nuclei over total DAPI nuclei per 40× field.

Statistical Analyses

Data were analyzed either by one-way analysis of variance (ANOVA) followed by Dunnett post hoc analysis or two-way ANOVA with a Bonferroni post test using Prism Ver 4.0 (GraphPad Software, San Diego, CA).

Results

CVX-045 Inhibits Angiogenesis In Vitro *and* In Vivo

In Boyden chamber experiments, CVX-045 inhibited the FBS-induced migration of endothelial cells with a half-maximal inhibitory concentration (IC_{50}) value of 1 to 10 nM (Figure 1*A*). The antiangiogenic activity of CVX-045 was further evaluated in a Matrigel plug assay. CVX-045 significantly attenuated the angiogenic response to FGF-2 by ~31% to 36% at a dose of 1 mg/kg or less (Figure 1*B*). These data demonstrate that CVX-045 had antiangiogenic activity.

CVX-045 Reduces Viable Tumor Volume and Microvessel Density in Tumor Xenografts

The β half-life of CVX-045 in mice was approximately 50 hours (Table 1), suggesting that weekly dosing would be an effective schedule for treating xenografts. Weekly administration of CVX-045 at a dose of 10 mg/kg resulted in significant ($P < .05$, $n = 9$ per group) reductions in tumor growth rate of A431 epidermoid carcinoma xenografts and A549 lung adenocarcinoma xenografts (Figure 2, *A* and *B*). Histologic analysis of excised treated tumors demonstrated a significant reduction in viable tumor area in both A431 and A549 xenografts compared with untreated tumors (Figure 2, *C* and *D*). Furthermore, CVX-045 treatment caused a significant reduction ($P < .05$, $n = 9$ per group) in microvessel density in both A431 and A549 xenografts (Figure 2, *E* and *F*).

CVX-045 Induced Apoptosis in Tumors within 1 Hour of Administration

A549-bearing animals were treated with CVX-045 weekly at 30 mg/kg. Tumors were excised at various time points after drug administration and analyzed histologically for cleaved caspase 3 (apoptosis), CD31 (mvd), and PCNA (proliferation).

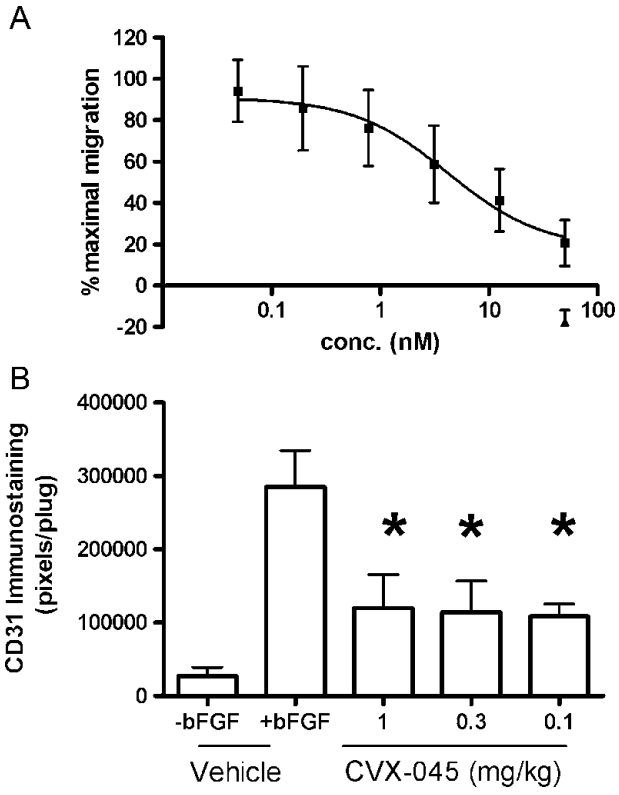

Figure 1. (A) CVX-045 (–■–) inhibits the serum-induced migration of endothelial cells. CVX-045 (–▲–) in the absence of FBS had no effect on endothelial cell migration. Values are mean ± SEM, $n = 4$. (B) CVX-045 significantly ($P < .05$, ANOVA, Dunnett post test, $n = 3$ per group) inhibits FGF-2–induced angiogenesis at doses of 0.1 to 1 mg/kg as determined by quantifying CD31 staining in a Matrigel plug assay.

CVX-045–treated tumors demonstrated visible apoptosis within 1 hour of drug administration when compared with PBS-treated tumors (Figure 3, *A* and *B*). Inspection of the histology images suggests that the initial apoptosis is seen within the endothelial cell compartment as demonstrated by the colocalization of cleaved caspase 3 and CD31 staining (Figure 3, *A–D*). From weeks 2 to 4, there is a collapse of the tumor cell compartment as indicated by the increase in cleaved caspase 3 staining, evident within the tumor cell compartment as opposed to the endothelial cell compartment (Figure 3, *E–H*). Quantification of the cleaved caspase 3 signal indicated that the increased level of apoptosis attained statistical significance at weeks 2 and 4 (Figure 4*A*). Quantification of the CD31 staining in these tumors demonstrated a decrease in microvessel density within 1 hour

Table 1. Pharmacokinetic Parameters of CVX-045 in Mice.

Species	AUC (h/μg per milliliter)	α t_{12} (h)	β t_{12} (h)	C_{max} (μg/ml)
Mouse	1177 (8.12)	1.60 (19.7)	53.05 (7.15)	119.4 (16.7)

Pharmacokinetic parameters of CVX-045 were derived from a two-compartment model (weighted $1/y^2$) calculated with the WinNonlin software after a single intravenous dose of CVX-045 (10 mg/kg) in male Swiss Webster mice. Sampling time points range from 5 minutes to 14 days. Data are expressed as the mean (%CV).

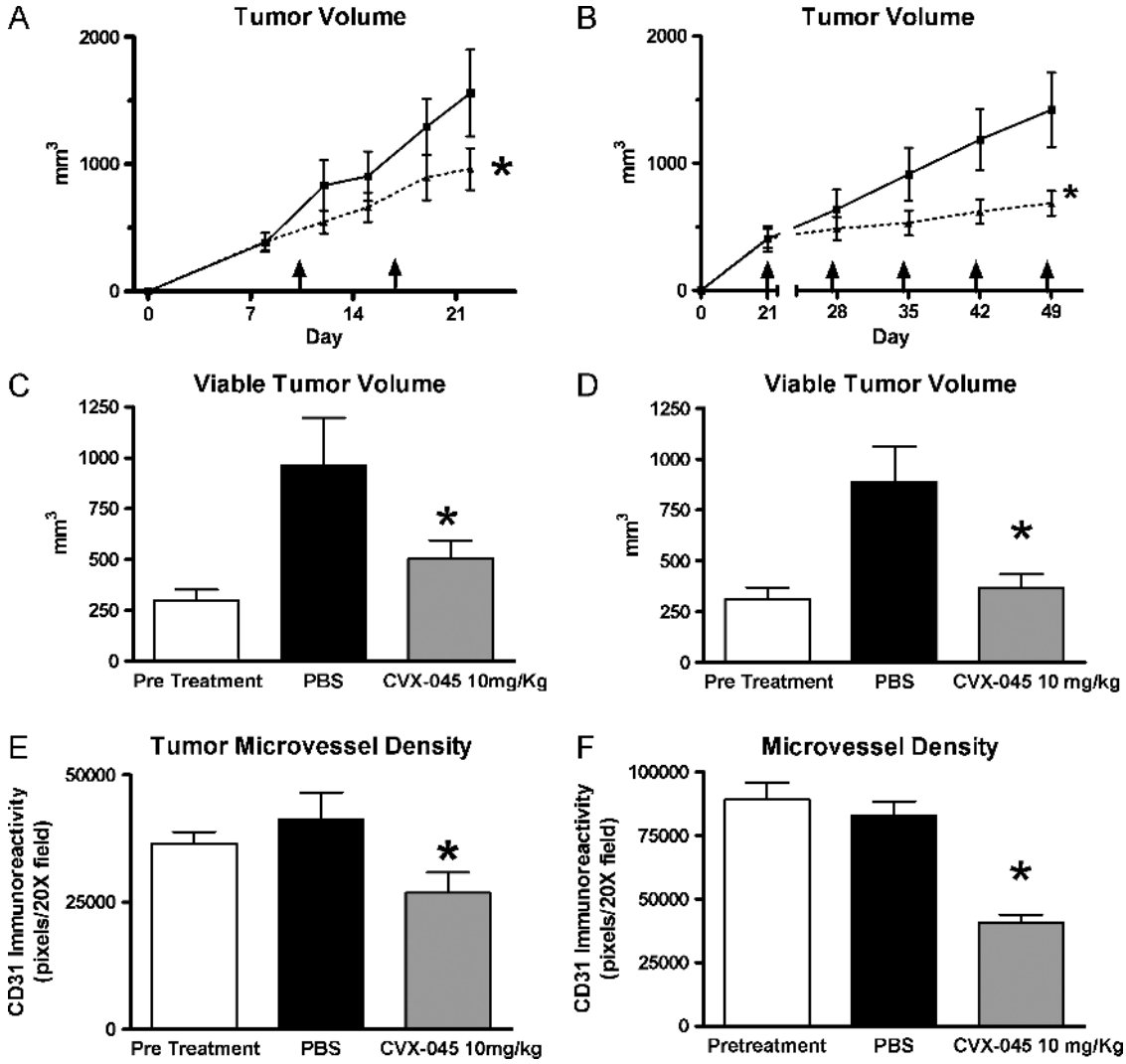

Figure 2. (A) CVX-045 (–▲–) inhibits growth of A431 xenograft at a dose of 10 mg/kg administered weekly. The reduction in tumor volume was statistically significant ($P < .05$, two-way ANOVA with Bonferroni correction, $n = 9$ per group) by day 21 when compared with the growth of vehicle-treated tumors (–■–). (B) CVX-045 (–▲–) inhibits growth of A549 xenograft at a dose of 10 mg/kg administered weekly. The reduction in tumor volume was statistically significant ($P < .05$, two-way ANOVA with Bonferroni correction, $n = 9$ per group) at day 49 when compared with the growth of vehicle-treated tumors (–■–). (C) CVX-045 treatment (10 mg/kg 1×/wk) significantly reduces ($P < .05$, one-way ANOVA, Newman-Keuls multiple comparison test, $n = 5$ per group) the viable tumor volume of A549 tumors when compared with PBS-treated tumors. (D) CVX-045 treatment (10 mg/kg 1×/wk) significantly reduces ($P < .05$, one-way ANOVA, Newman-Keuls multiple comparison test, $n = 5$ per group) the viable tumor volume of A431 tumors when compared with PBS-treated tumors. (E) CVX-045 treatment (10 mg/kg 1×/wk) significantly reduces ($P < .05$, one-way ANOVA, Newman-Keuls multiple comparison test, $n = 5$ per group) the microvessel density of A549 tumors when compared with PBS-treated tumors. (F) CVX-045 treatment (10 mg/kg 1×/wk) significantly reduces ($P < .05$, one-way ANOVA, Newman-Keuls multiple comparison test, $n = 5$ per group) the microvessel density of A431 tumors when compared with PBS-treated tumors.

of drug administration, attaining statistical significance by 2 weeks (Figure 4*B*). The level of proliferating cells, as quantified by PCNA staining, also showed a statistically significant reduction by week 4 (Figure 4*C*).

The effects of bevacizumab, dosed at 5 mg/kg twice weekly, to alter various tumor parameters such as apoptosis and mvd, were also assessed in the A549 model. These data are presented in Table 2.

CVX-045 Improves the Efficacy of Chemotherapy and Targeted Therapy

The efficacy of CVX-045 in combination with chemotherapy and targeted therapy was tested using either standard tumor xenograft growth rate experiments or "pseudomortality" experimental design, in which treatment groups were allowed to attain a predetermined tumor volume and the time to attain that volume was recorded.

When tested in a standard growth rate experiment, neither CVX-045 at a dose of 30 mg/kg weekly nor 5-FU at a dose of 100 mg/kg weekly significantly affected the growth rate of HT-29 colorectal carcinoma xenografts (Figure 5*A*). However, the combination of these drugs did result in a significant reduction in tumor growth rate ($P <$ .01) compared with vehicle alone (Figure 5*A*).

When tested in a pseudomortality experiment, CPT-11 at 100 mg/kg weekly had efficacy against HT-29 xenografts, increasing the time to attain 2000 mm^3 from 27 to 39 days. This efficacy was greatly improved

when coadministered with CVX-045 (Figure 5*B*), the combination did not attain a tumor volume of 2000 mm^3 until day 56 of therapy (Figure 5*B*).

Combination of CVX-045 and sunitinib were also tested in animal models using HT-29 xenografts. Both CVX-045 at 30 mg/kg weekly and sunitinib at 15 mg/kg daily were ineffective in reducing tumor growth rate (Figure 5*C*), whereas the combination of CVX-045 and sunitinib significantly ($P = .0006$) reduced tumor rate compared with vehicle (Figure 5*C*). Tumors in animals receiving this combination took 40 days to reach a volume of 1000 mm^3 compared with 26 days for PBS-treated controls.

Discussion

A TSP-1 mimetic CovX-body (CVX-045) was produced by covalently linking a TSP-1 mimetic pharmacophore to a proprietary antibody. The TSP-1 mimetic pharmacophore contains a reactive group that is specifically recognized by the antibody Fab active site reactive lysine and forms an irreversible covalent bond to create CVX-045. Chemically

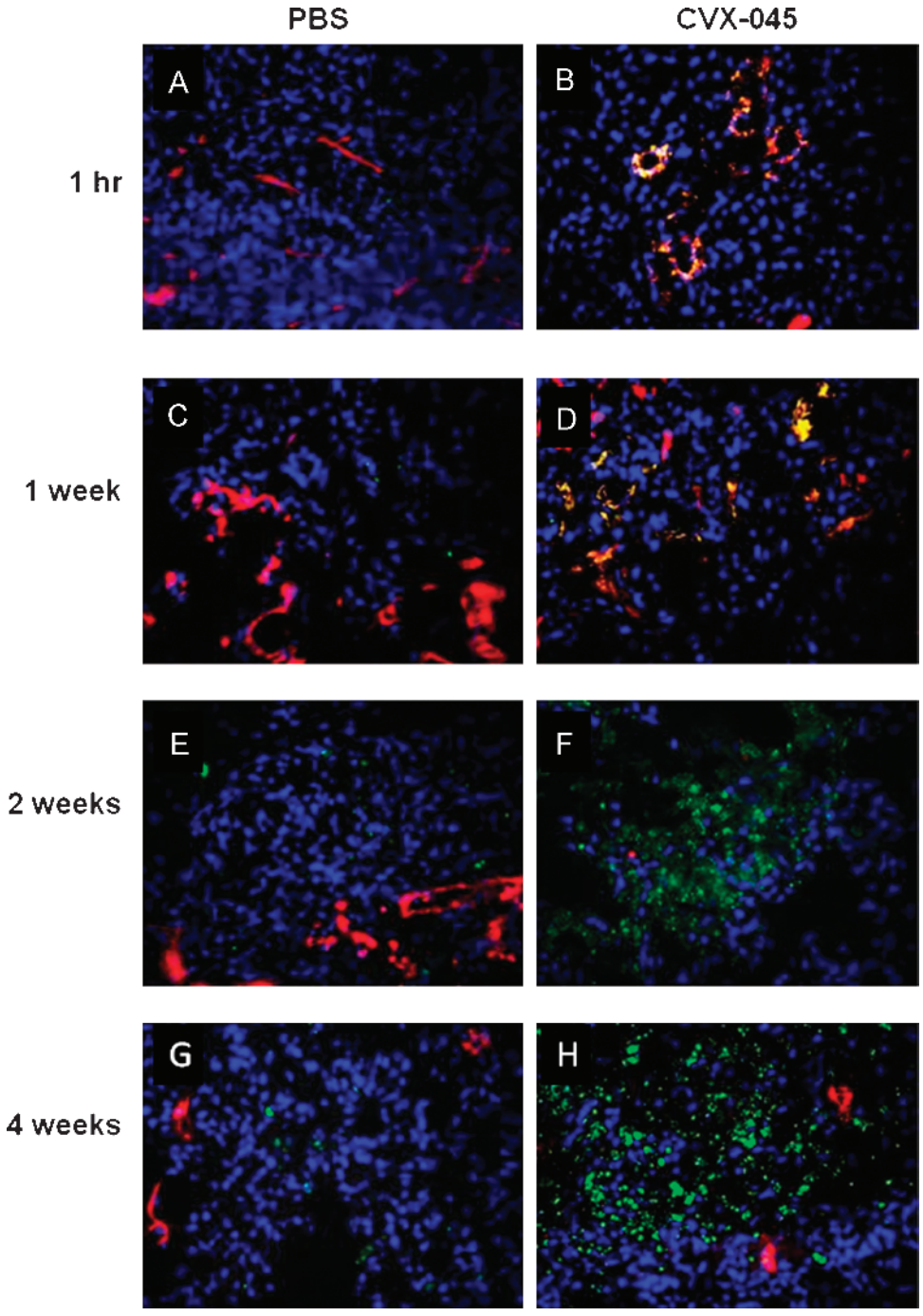

Figure 3. (A–H) A549 tumors, treated with either PBS or CVX-045 (30 mg/kg 1×/wk), were excised at the time points indicated and sections stained for CD31 (red) to indicate endothelial cells or cleaved caspase 3 (green) to indicate apoptotic cells. Tumor cells were stained with DAPI (blue). Separate images were merged to give yellow regions where red and green overlay, indicating apoptotic endothelial cells.

conjugating peptides to the scaffold antibody has been demonstrated to enhance the potency of the peptide (possibly due to bivalency) and to enhance the PK of the pharmacophore peptide [17,18]. Thus, generating a CovX-body from a peptide allows the peptide to be administered on an antibody-like schedule.

CVX-045 is a potent inhibitor of endothelial cell migration, as measured in a Boyden chamber. CVX-045 is also a potent antiangiogenic as measured in the Matrigel plug assay inhibiting angiogenesis at doses as low as 0.1 mg/kg 1×/wk.

Other laboratories have shown that pharmacophores derived from TSP-1 domains retained antiangiogenic function and could inhibit tumor growth in a variety of animal models, although these small-molecular weight pharmacophores must be administered frequently and at high doses. CVX-045 has the PK profile of an antibody, demonstrating a β $t_{1/2}$ of 50 hours in mice and approximately 80 hours in nonhuman primates. The antiangiogenic potency and PK profile indicated that CVX-045 should have efficacy in preclinical tumor models when dosed weekly.

CVX-045 was able to significantly reduce the growth rate of both the squamous cell carcinoma A431 and the lung adenocarcinoma A549 when administered intravenously at 10 mg/kg weekly. Histologic analysis of excised tumors showed that CVX-045 caused a significant reduction in both viable tumor volume and microvessel density by the end of the study.

It is well established that decreased microvessel density, although indicative of an antiangiogenic effect is not sufficient for complete tumor volume reduction in hypoxia-resistant tumor models. Moreover, microvessel density is not a measure of the angiogenic dependence of a tumor but, to a large degree, reflects the metabolic burden of the supported tumor cells. A minimum vessel density is determined by tumor cell metabolic demand, but vessel density can exceed the metabolic requirements of a tumor. Thus, a therapy regimen that reduces microvessel density may not have a complete impact on tumor volume but may have a partial impact on viable tumor area.

There is an observed decrease in viable tumor volume in A431 and A549 tumor xenografts in response to CVX-045 therapy. This is similar to the observation from other laboratories that have shown that overexpression of TSP-1 in genetically engineered tumor cell lines is also characterized by an increase in tumor necrosis in A431 and other xenograft models [19]. These observations fit with the mechanism of TSP-1 as an antiangiogenic molecule. If TSP-1 is causing a decrease in angiogenesis within the tumor, this would manifest as necrotic areas, resulting from nutrient and oxygen deprivation.

A further study of the efficacy of CVX-045 in the A549 xenograft model revealed that CVX-045 has an observable apoptotic effect on tumor vasculature within 1 hour of administration, and this increase in apoptosis was statistically significant at 2 weeks. Examination of the stained tumor sections reveals that by week 1 of therapy, the apoptosis is apparently confined to the tumor vasculature, whereas by week 4, the increased apoptosis is seen in nonendothelial cells within the tumor. This indicates that CVX-045 is having an immediate effect on the vascular compartment of the tumor resulting in acute

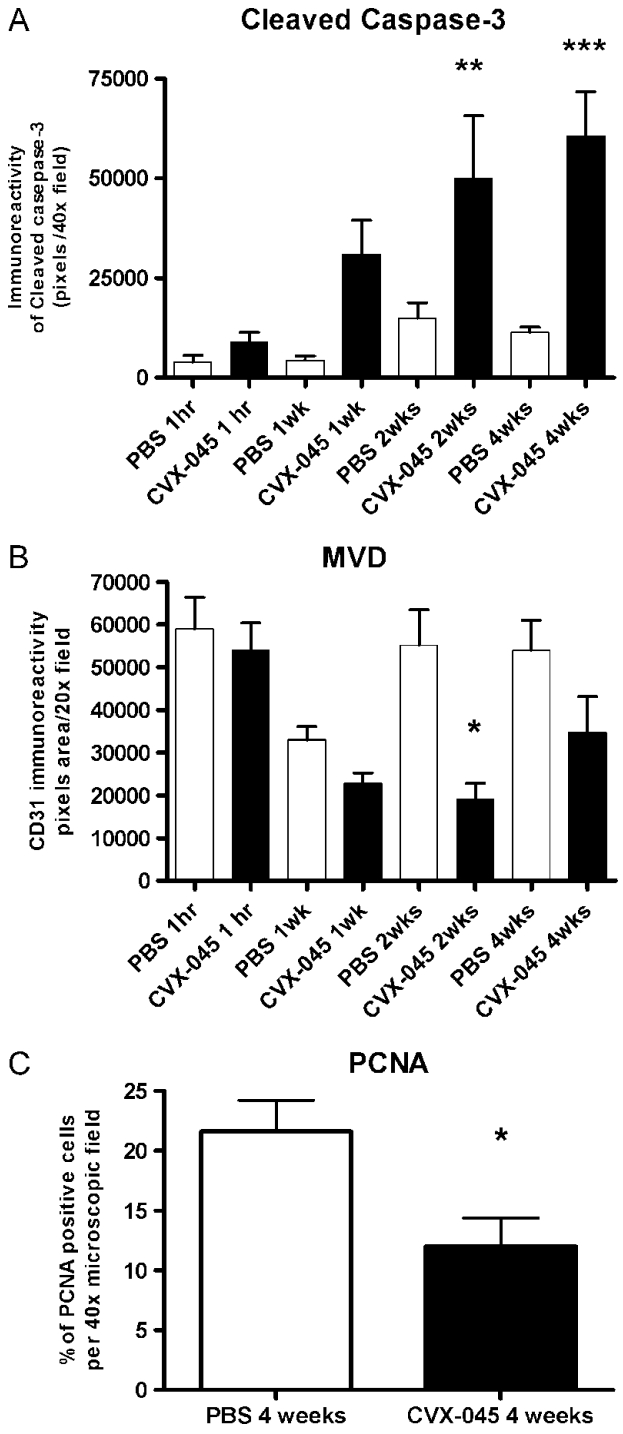

Figure 4. (A) Levels of apoptotic cells (as indicated by cleaved caspase 3 staining) were quantified in A549 tumor sections obtained from tumors excised at various time points after treatment with CVX-045 (30 mg/kg 1×/wk). There was a significant ($P < .01$, ANOVA, Tukey multiple comparison posttest, $n = 5$ per group) increase in apoptosis of CVX-045–treated tumors compared with PBS-treated tumors at 2 and 4 weeks. (B) Microvessel density (as indicated by CD31 reactivity) was quantified in A549 tumor sections obtained from tumors excised at various time points after treatment with CVX-045 (30 mg/kg 1×/wk). There was a significant ($P < .05$, ANOVA, Tukey multiple comparison posttest, $n = 5$ per group) decrease in microvessel density observable between PBS-treated and CVX-045–treated tumors at 2 weeks. (C) The percentage of PCNA-positive cells was quantified in A549 tumors after 4 weeks of CVX-045 treatment (30 mg/kg 1×/wk). A significant ($P < .05$, Mann-Whitney test, $n = 5$ per group) decrease in PCNA staining was observed in the CVX-045–treated group at 4 weeks.

Table 2. Comparison of the Effects of CVX-045 and Bevacizumab on Measurable End Points in the A549 Model.

Treatment	End Points	1 wk	2 wk	4 wk
PBS				
CVX-045 (30 mg/kg 1×/wk)	Apoptosis		*	†
	MVD		†	
Bevacizumab (5 mg/kg 2×/wk)	Apoptosis	*		†
	MVD		†	†

Apoptosis and MVD were measured as described. Statistical differences were determined using ANOVA with a Bonferroni post test to compare test samples to time-matched PBS-treated controls. MVD indicates microvessel density.
*$P < .05$.
†$P < .001$.

collapse of the vasculature. More its chronic effects are the subsequent apoptosis of tumor cells that are being deprived of oxygen and nutrients. This does indicate that *in vivo*, CVX-045 is eliciting its antitumorigenic effects via an antiangiogenic mechanism. Previously, we have demonstrated that a less mature iteration of a thrombospondin mimetic CovX-Body (CVX-22) was selectively active against proliferating endothelial cells within a tumor [20]. Specifically, CVX-22 reduced the numbers of activated VEGF receptor 2–positive tumor endothelial cells, a subset of endothelial cells that contain most of the mitotically active endothelial cells.

Assessment of PCNA staining at week 4 of therapy revealed a significant reduction in proliferation within the tumor, providing further evidence that CVX-045 antitumor effects are not acute.

CVX-045, in common with most antiangiogenic agents, was able to reduce microvessel density and decrease the viable tumor volume of xenografts in single agent studies. However, it is well appreciated that tumors can be partially resistant to antiangiogenic therapy owing to the induction of gene expression as a consequence of hypoxia. All antiangiogenic agents thus far approved for clinical use are given in combination with either chemotherapy or stand-of-care targeted therapies. Our experience with HT-29 colorectal adenocarcinoma suggested that this cell line was essentially resistant to CVX-045 monotherapy. We decided to test CVX-045 in combination with 5-FU, CPT-11, and sunitinib in this model to test whether a combination of modalities could be effective in inhibiting tumor growth rate.

We tested these combinations in either classic growth rate models or pseudomortality models, where the time taken by a treatment group to reach a predetermined tumor volume is recorded and compared with vehicle-treated groups. Although the growth rate of HT-29 xenografts was unaffected by CVX-045, 5-FU, or sunitinib monotherapy, the combination of CVX-045 and 5-FU produced a significant reduction in tumor volume by day 30 of treatment. The combination of CVX-045 and sunitinib was also more effective than either monotherapy alone. CPT-11 therapy was effective in inhibiting the growth rate of HT-29 xenografts, but the combination of CVX-045 and CPT-11 was even more effective. These data suggest that CVX-045 combines well with other modalities, including antimetabolites, topoisomerase II inhibitors, and tyrosine kinase inhibitors.

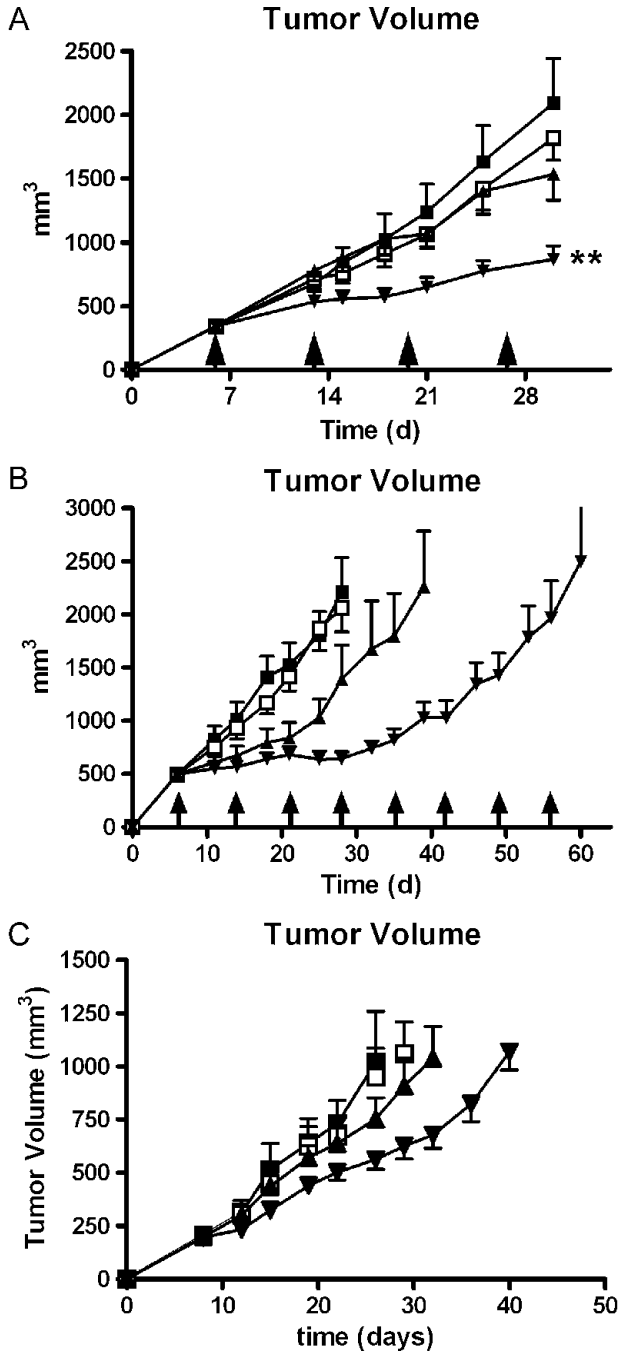

Figure 5. (A) Neither CVX-045 (–□–) administered at 30 mg/kg 1×/wk nor 5-FU (–▲–) administered at 100 mg/kg intraperitoneally 1×/wk significantly inhibit the growth of HT-29 xenograft when compared with the growth rate of PBS treated tumors (–■–). A combination of these two drugs (–▼–) does inhibit the growth rate of HT-29 tumors by day 29. The reduction in tumor volume was statistically significant ($P < .05$, one-way ANOVA, $n = 9$ per group) by day 29 when compared with the growth of vehicle-treated tumors (–■–). (B) CVX-045 (–□–) administered at 30 mg/kg 1×/wk did not significantly inhibit the growth of HT-29 xenograft when compared with the growth rate of PBS-treated tumors (–■–). CPT-11, administered at 100 mg/kg 1×/wk intraperitoneally, was able to significantly ($P < .001$, two-way ANOVA, $n = 9$ per group) inhibit the growth of these tumors (–▲–). A combination of these two drugs (–▼–) further significantly ($P < .001$, two-way ANOVA, $n = 9$ per group) inhibited the growth rate of HT-29 tumors. (C) Neither CVX-045 (–□–) administered at 30 mg/kg 1×/wk or sunitinib (–▲–) administered at 15 mg/kg per os daily significantly inhibit the growth of HT-29 xenograft when compared with the growth rate of PBS-treated tumors (–■–). A combination of these two drugs (–▼–) does significantly ($P < .001$, two-way ANOVA, $n = 9$ per group) inhibit the growth rate of HT-29 tumors.

CVX-045 has recently completed a phase 1 clinical trial [16]. Eighteen patients with advanced solid tumors and no known bleeding risk received CVX-045 administered in three-patient cohorts (0.3, 1, 3, 6, 12, and 18 mg/kg) by once-weekly intravenous infusions. Common adverse events (grade 1-2) included gastrointestinal anemia, headache, fatigue, and general muscle weakness. Dynamic contrast enhanced-magnetic resonance imaging showed effects on flow (21%–42% decrease in K_{trans}) but not permeability (AUCBN(90)) in two of three patients in the 12-mg/kg group and in one patient in the 6-mg/kg group. There was an unconfirmed partial response in 1 patient with liver metastases and stable disease in 5 of 12 patients. Of 18 patients, 1 (6%) was potentially positive for an immune response to study drug on cycle 1, day 1. All subsequent test results were negative. All other patients with test results reported were negative. It was concluded that CVX-045 was a well-tolerated new therapy targeting angiogenesis by a novel pathway with preliminary evidence by dynamic contrast enhanced-magnetic resonance imaging and RECIST to suggest biologic activity in the clinic.

It is well appreciated that novel efficacious antiangiogenic therapies will find a place in the clinic in combination with standard-of-care therapies. CVX-045 is an antiangiogenic molecule. Antiangiogenic effects are a phenomenon that can be driven by different molecular mechanisms. Therapies can either inhibit angiogenesis or promote antiangiogenesis by altering the angiogenic switch. Bevacizumab obviously traps VEGF and, in doing so, inhibits angiogenesis, whereas CVX-045 is hypothesized to promote antiangiogenesis. Within the modalities that inhibit VEGF-driven angiogenesis are drugs that block signaling from inside the cell, such as sunitinib. Each of these mechanisms may offer advantages and disadvantages when used in combination therapy regimens. It is known, for example, that adding sunitinib to bevacizumab can result in increased toxicities with no discernable benefit [21,22]. When combining antiangiogenic therapies with other modalities, it may be that the underlying mechanism driving the antiangiogenic effects is the arbiter of a safe and effective combination. Drugs such as CVX-045 may offer a combination option not available to bevacizumab owing to underlying differences in the molecular mechanism. The preclinical data presented here suggest possible effective combinations for CVX-045 in the future.

References

[1] Folkman J (2004). Endogenous angiogenesis inhibitors. *APMIS* **112**, 496–507.

[2] Fraser HM and Lunn SF (2000). Angiogenesis and its control in the female reproductive system. *Br Med Bull* **56**, 787–797.

[3] Bergers G and Benjamin LE (2003). Tumorigenesis and the angiogenic switch. *Nat Rev Cancer* **3**, 401–410.

[4] Pirie-Shepherd SR (2003). Regulation of angiogenesis by the hemostatic system. *Front Biosci* **8**, d286–d293.

[5] Thompson WD, Harvey JA, Kazmi MA, and Stout AJ (1991). Fibrinolysis and angiogenesis in wound healing. *J Pathol* **165**, 311–318.

[6] Dvorak HF (1986). Tumors: wounds that do not heal. Similarities between tumor stroma generation and wound healing. *N Engl J Med* **315**, 1650–1659.

[7] Folkman J (1971). Tumor angiogenesis: therapeutic implications. *N Engl J Med* **285**, 1182–1186.

[8] Hurwitz HI, Fehrenbacher L, Hainsworth JD, Heim W, Berlin J, Holmgren E, Hambleton J, Novotny WF, and Kabbinavar F (2005). Bevacizumab in combination with fluorouracil and leucovorin: an active regimen for first-line metastatic colorectal cancer. *J Clin Oncol* **23**, 3502–3508.

[9] Motzer RJ, Michaelson MD, Redman BG, Hudes GR, Wilding G, Figlin RA, Ginsberg MS, Kim ST, Baum CM, DePrimo SE, et al. (2006). Activity of SU11248, a multitargeted inhibitor of vascular endothelial growth factor receptor and platelet-derived growth factor receptor, in patients with metastatic renal cell carcinoma. *J Clin Oncol* **24**, 16–24.

[10] Lawler J (2002). Thrombospondin-1 as an endogenous inhibitor of angiogenesis and tumor growth. *J Cell Mol Med* **6**, 1–12.

[11] Allegrini G, Goulette FA, Darnowski JW, and Calabresi P (2004). Thrombospondin-1 plus irinotecan: a novel antiangiogenic-chemotherapeutic combination that inhibits the growth of advanced human colon tumor xenografts in mice. *Cancer Chemother Pharmacol* **53**, 261–266.

[12] Lawler J and Hynes RO (1986). The structure of human thrombospondins, an adhesive glycoprotein with multiple calcium binding sites and homologies with several different proteins. *J Cell Biol* **103**, 1635–1648.

[13] Dawson DW, Volpert OV, Pearce SF, Schneider AJ, Silverstein RL, Henkin J, and Bouck NP (1999). Three distinct D-amino acid substitutions confer potent antiangiogenic activity on an inactive peptide derived from a thrombospondin-1 type 1 repeat. *Mol Pharmacol* **55**, 332–338.

[14] Reiher FK, Volpert OV, Jimenez B, Crawford SE, Dinney CP, Henkin J, Haviv F, Bouck NP, and Campbell SC (2002). Inhibition of tumor growth by systemic treatment with thrombospondin-1 peptide mimetics. *Int J Cancer* **98**, 682–689.

[15] Mendelson DS, Dinolfo M, Cohen RB, Rosen LS, Gordon MS, Byrnes B, Bear I, and Schoenfeld SL (2008). First-in-human dose escalation safety and pharmacokinetic (PK) trial of a novel intravenous (IV) thrombospondin-1 (TSP-1) mimetic humanized monoclonal CovX Body (CVX-045) in patients (pts) with advanced solid tumors. *J Clin Oncol* **26**, Abstract 3524.

[16] Polverini PJ, Bouck NP, and Rastinejad F (1991). Assay and purification of naturally occurring inhibitor of angiogenesis. *Methods Enzymol* **198**, 440–450.

[17] Bower KE, Lam SN, Oates BD, Del Rosario JR, Corner E, Osothprarop TF, Kinhikar AG, Hoye JA, Preston RR, Murphy RE, et al. (2011). Evolution of potent and stable placental-growth-factor-1–targeting CovX-bodies from phage display peptide discovery. *J Med Chem* **54**, 1256–1265.

[18] Huang H, Lai JY, Do J, Liu D, Li L, Del Rosario J, Doppalapudi VR, Pirie-Shepherd S, Levin N, Bradshaw C, et al. (2011). Specifically targeting angiopoietin-2 inhibits angiogenesis, Tie2-expressing monocyte infiltration, and tumor growth. *Clin Cancer Res* **17**, 1001–1011.

[19] Streit M, Velasco P, Brown LF, Skobe M, Richard L, Riccardi L, Lawler J, and Detmar M (1999). Overexpression of thrombospondin-1 decreases angiogenesis and inhibits the growth of human cutaneous squamous cell carcinomas. *Am J Pathol* **155**, 441–452.

[20] Coronella J, Li L, Johnson K, Pirie-Shepherd S, Roxas G, and Levin N (2009). Selective activity against proliferating tumor endothelial cells by CVX-22, a thrombospondin-1 mimetic CovX-Body. *Anticancer Res* **29**, 2243–2252.

[21] Mayer EL, Dhakil S, Patel T, Sundaram S, Fabian C, Kozloff M, Qamar R, Volterra F, Parmar H, Samant M, et al. (2010). SABRE-B: an evaluation of paclitaxel and bevacizumab with or without sunitinib as first-line treatment of metastatic breast cancer. *Ann Oncol* **21**, 2370–2376.

[22] Socinski MA, Scappaticci FA, Samant M, Kolb MM, and Kozloff MF (2010). Safety and efficacy of combining sunitinib with bevacizumab + paclitaxel/carboplatin in non–small cell lung cancer. *J Thorac Oncol* **5**, 354–360.